Confined Water-Assistant Thermal Response of Graphene-Oxide

Heterostructure and Its Enabled Mechanical Sensors for Load Sensing and

Mode Differentiating

Yuan Gao, Yue Zhang, and Baoxing Xu

Department of Mechanical and Aerospace Engineering, University of Virginia,

Charlottesville, VA 22904, USA

* Corresponding author: bx4c@virginia.edu

Abstract

Mechanically responsive features are essential in devising mechanical sensors capable

of sensing and differentiating loadings. We present a heterostructure composed of

bilayer graphene oxides and confined water as a mechanical sensor that enables the

detection and differentiation of tension, compression, pressure and bending. Guided by

molecular simulations, we demonstrate that the thermal transport across solid-liquid

interfaces is sensitive to loading modes owing to the reversible response of hydrogen

bonding networks between confined water molecules and graphene oxides, and

quantitatively elucidate the thermal transport mechanism by correlating thermal

conductance, number and distribution of hydrogen bonds and interfacial energy with

mechanical loadings. Such structure-enabled mechanical sensor with contrasting

thermal response to different loading modes is devised to exemplify robustness of

sensing functions. These results lay a foundation for rational designs of mechanical

sensors that leverage the thermal response of solid-liquid systems, beyond the current

strategy relying on electrical properties of sole solids.

Keywords: graphene oxide heterostructure, confined liquid, thermal transport,

hydrogen bonds, mechanical loading mode

1

1. Introduction

Rational designs of flexible functional devices with the capability of sensing and differentiating multiple mechanical loading modes are of fundamental importance for the development of next-generation electronic devices, 1 such as e-skin2 and humanoids robotics³ to track and mimic human intents associated with multiple human modalities in human-machine interactions and to record human daily exercises in healthcare monitoring and disease diagnosis. To achieve such design, sensor components with well-defined functions and structures are usually designed individually, fabricated and integrated on various substrates.⁴ In particular, a careful material selection and/or structural integration, ranging from the employment of individual functional material elements to the creation of composite materials,⁵ and from bioinspired structural designs to topological optimization designs, 6 is required to improve the sensing sensitivity and loading mode identification. Typical examples include interlocked arrays of nanofibers for highly sensitive strain gauge sensors, ⁷ layered assemblies of strain and pressure sensors in skin-like multifunctional sensors,⁸ and bioinspired cracktype sensors in enhanced strain measurements. 9 The operating efficiency of these devices is another critical consideration and usually is based on measurements of the electrical resistivity in response to mechanical loading conditions. 10 Widespread adoption of such mechanism-driven sensors, however, is limited by surrounding environments with the coupling of multiple aspects. For example, minimizing the effect of temperature is challenging the designs and material selections in mechanical sensors because the electrical resistance of sensor materials is sensitive to temperature, ¹¹ similar to that with mechanical loading. In addition, the reduction of device size that will allow increasing numbers of sensing pixels per integrated area will significantly challenge thermal management, in particular, in nanosized sensor devices. 12

Heterostructures, composed of layered two-dimensional nanomaterials, ¹³⁻¹⁴ have a well-established set of mechanical flexibilities ¹⁵⁻¹⁶ and are emerging as an attractive structural platform for flexible mechanical sensors. The programmable pattern design to individual layer components ¹⁷ and the regulatory interlayer distance ¹⁸ further foster

the exploration of unprecedented properties that are capable of responding to external environments and stimuli means, which in turn can be leveraged for sensor and functional material designs. For example, recent work shows that heterostructures assembled by graphene oxide exhibit ten times higher of mechanical toughness than that of natural nacre due to the enhanced interlayer cohesion by surface functional groups.¹⁹ The direct coordination of heterostructures with polar materials such as cellulose nanocrystals facilitates assembly of their nanocomposites with a highly ordered morphology and improves the response sensitivity to external environments such as humidity sensor.²⁰ These sensors enabled by heterostructures, similar to the ones enabled by metals and semiconductors, rely critically on the change in electrical resistance and possess limited ability to minimize the effect of temperatures in the use for mechanical loading sensing and mode differentiation.

Here, we explore a bilayer graphene-oxide (GO) heterostructure with liquid water molecules confined in the interlayer. Guided by the full-scale atomistic modeling and dynamics simulations, we present a design strategy of mechanical sensor that is based on the unique thermal response to four typical mechanical loading modes including tension, compression, pressure and bending. Specifically, we investigate the thermal transport across the solid-confined liquid interface of bilayer graphene-oxide heterostructure and reveal that its mechanism is closely related to the reversible dynamics of hydrogen bonds between graphene oxide-confined water and graphene oxide-graphene oxide. Fundamental studies of the correlation between thermal conductance of heterostructures and applied mechanical loadings demonstrate a contrasting thermal response to mechanical loading modes. Demonstration application of such heterostructure enabled mechanical sensor is exemplified to illustrate its sensing function and mode identification through the determination of temperature change in response to mechanical loadings. The sensing mechanisms of based-on-changes in the thermal response of confined liquid water-heterostructure systems from mechanical deformations reported here strategically establish a general rationale for designing flexible mechanical sensors capable of sensing multiple mechanical loadings with a clear mode differentiation, and offer insights in future functional sensor designs by leveraging solid-confined liquid interactions.

2. Computational Modeling and Methodology

2.1. Atomistic modeling and molecular dynamics simulations. All the molecular dynamics computations were carried out with LAMMPS package. The time step was set as 0.5 fs. The covalently bonded interactions within graphene oxide were modeled by OPLS-AA force field that proves to reproduce both mechanical and thermal transport properties of graphene oxide. The widely adopted SPC/E model was utilized to describe the behavior of water molecules. The non-bonded van der Waals interactions were modeled by Lennard-Jones potential, and the particle-particle-particle-mesh (PPPM) with a root mean of 0.0001 was applied to evaluate the Coulomb interactions between charged atoms. This combined force field to non-bonded interactions has proved to generate similar cohesive relations of H-bonds (**Figure S1**) as those reflected by ReaxFF potential. The GO-water heterostructure was set between hot and cold substrates which are represented by GO layers with the same degree of oxidation. The periodic condition was applied in the in-plane direction of graphene oxide (x and y-direction) and non-periodic boundary condition was applied in the cross-plane direction (z-direction).

The system was first relaxed in the NPT ensemble at a constant temperature of 300 K maintained by Nose-Hoover method for 1 ns. Next, NVT ensemble was applied to further optimize the heterostructure at 300K for another 1 ns. To calculate the thermal conductance, the reverse nonequilibrium molecular dynamics was employed, detailed as: a constant amount of kinetic energy was added to/subtracted from the hot and the cold substrates by rescaling the velocity of atoms in substrates at each time step to generate a constant heat flow. To achieve an equal initial temperature difference at the heterojunction, $\Delta T_0 = 60$ K that is usually employed in simulations,²⁷ the heat flow ranging from 0.5 nW to 0.7 nW for different computational systems was applied. This

process continued for 4 ns and the thermal conductance was calculated via $G = q/\Delta T$ from the temperature data obtained during the last 2 ns. The temperature fluctuation in upper and lower GO layers in the simulations was reflected by error bars in data plots.

To apply an external tensile or compressive strain, a uniform displacement at a strain rate $\varepsilon_x = \pm 0.5$ ns⁻¹ which can be approximately considered as a quasistatic manner was introduced to the system every 1000 time steps by remapping the x coordinates of atoms. In particular, consider these pristine graphene-oxide layers whose failure strain is around $15\%^{28,29}$, the tensile strain of no more than 10% was focused. To introduce external pressure to the system, an external yet equal force in z-direction was applied to the carbon atoms in the substrate. To apply a bending deformation, non-periodic boundary condition was applied to replace the periodic one in the x-direction. Besides, a neutral plane was assumed to locate in the middle of the centers of masses of two GO layers in heterostructures, 30 the coordinates of atoms could be predicted by continuum mechanics and remapped. In the simulations, the atoms on curved edges were fixed and the system was further relaxed for 1 ns before calculations on thermal transport. This procedure of applying bending deformation is similar to that of the popular targeted molecular mechanics (TMM) method. 31

2.2. Calculation of thermal transport by GO-GO H-bonds and GO-W H-bonds.

The thermal transport could be decoupled by calculating the power exchange in the lower graphene oxide with upper graphene oxide as well as water molecules according to $q_{GO-GO}=0.5(\sum_{i\in upperGO,j\in lowerGO}F_{ij}\cdot v_j-\sum_{i\in upperGO,j\in lowerGO}F_{ji}\cdot v_i)$, 32 where F_{ij} denotes the force vector exerted on atom j by atom i, and v_j represents the velocity vector of atom j. Similarly, $q_{GO-W}=0.5(\sum_{i\in water,j\in lowerGO}F_{ij}\cdot v_j-\sum_{i\in water,j\in lowerGO}F_{ji}\cdot v_i)$ can be obtained. Their contributions to the thermal conductance between upper and lower GO layers was further obtained by $G_{GO-GO}=q_{GO-GO}/\Delta T$ and $G_{GO-W}=q_{GO-W}/\Delta T$.

2.3. Calculation of phonon spectra and hydrogen bonds. The phonon spectra were obtained by performing fast Fourier transform on the velocity autocorrelation function according to $PS(\omega) = 1/\sqrt{2\pi} \int_0^\infty e^{-i\omega t} \frac{\langle v(t) \cdot v(0) \rangle}{\langle v(0) \cdot v(0) \rangle} d\omega$, where ω is the angular frequency and v(t) is the atomic velocity vector at time t. The symbol < > represents the average over atoms being concerned.

The hydrogen bonds in the system were identified according to two criteria associated with the geometry of the donor and acceptor. First, the H···O distance should not exceed 0.24 nm to encompass the first solvation shell in the radial distribution functions and is used for both water—water and water—functional group interactions.³³ Second, the H-O···O angle should be less than 30 degrees, which is usually applied to identify H-bonds in the systems enabled by GO and water molecules.³⁴ The amount of H-bonds in a specific system was obtained by calculating the number of H-bonds in 100 timeframes in the last 1 ns during the simulations.

3. Results and Discussion

3.1. Thermal conductance of bilayer graphene oxide (GO)-confined water heterostructures and its response to mechanical loading. Figure 1a depicts the schematic of the graphene oxide (GO)-confined water heterostructure. The dimension was l = 6.15 nm in length and w = 6.39 nm in width, and more details of the modeling can be found in the Computational Modeling and Methodology section. The two GO layers were decorated with equal numbers of randomly distributed epoxy and hydroxyl functional groups.²³ This surface functionalization led to two different degrees of oxidation p (=0.4 and 0.5), which is defined as the ratio of the number of functional groups to the number of carbon atoms in a GO layer. Various numbers of water molecules are confined between these two GO layers, and is represented by the weight ratio, $wt = m_{water}/m_{GO}$, where m_{water} and m_{GO} are the mass of water molecules and a single graphene oxide layer, respectively, and wt usually changes

from 0 to 25%. A constant heat flow q from the upper GO layer to the lower GO layer was applied to study the thermal transport properties of the heterostructure system (see Computational Modeling and Methodology section). Figure 1b presents the thermal conductance G of heterostructures as a function of water content. In the absence of confined water, G is 10.24 pW/K for the heterostructure with p = 0.5, which is higher than the conductance 7.71 pW/K of the heterostructure with p = 0.4. This relative higher G with p = 0.5 remains when wt increases to 25% due to the stronger atomic interactions provided by more functional groups at molecular junctions. 18 As the water content increases, G shows an increase until wt reaches 10%, followed by a decrease as the water content continuously increases. Such variation is more obvious at a higher p = (0.5) due to more functional groups in GO layers, which will potentially benefit the formation of GO-water hydrogen (H)-bonds as both donors and acceptors.²⁶ For the heterostructure, two types of H-bonds will be formed in the interlayer. One results from the interactions of the functional groups between GO layers, referred to as GO-GO H-bonds, as marked in red dash lines in the atomic schematics in Figure 1c, and the other governs the coordination between GO and confined water molecules, referred to as GO-W H-bonds, marked by the blue dash lines in Figure 1c. Further analysis shows that the contribution of van der Waals interaction associated with these two types of H-bonds to thermal transport is >90% and the effect of electrostatic interaction on thermal transport can be neglected (Figure S2). Consequently, the interactions associated with these two H-bonds can be considered to serve as two dominant paths of thermal transport across the interface, analogical to a circuit model, as illustrated in Figure 1c. By decoupling the heat flow (see Computational Modeling and Methodology section), Figure 1d gives the contribution of thermal transport along these two corresponding transfer routes, where G_{GO-GO} and G_{GO-W} represent the thermal conductance with the transport path from upper GO to lower GO via GO-GO H-bonds and from upper GO to water molecules and then to lower GO via GO-W H-bonds, respectively. With the increasing of the confined water molecules between GO layers, the equilibrium distance between two GO layers increases (Figure S3), weakening firsthand interactions between GO layers,

and thus leading to a reduction of GO-GO H-bonds and a lower G_{GO-GO} , as observed in Fig. 1d. By contrast, the interaction between GO and water molecules is enhanced through GO-W H-bonds, thus promoting G_{GO-W} .

Given the stronger ability to form H-bonds in the heterostructure with p = 0.5, we will take it as a material design platform to exemplify the response of thermal transport to external applied mechanical loadings. Four typical mechanical loading modes of in-plane tension and compression and out-of-plane pressure and bending will be investigated and their realization in atomistic modeling can be found in Computational Modeling and Methodology section. Figure 2a presents the effect of inplane external tensile loading ε_t on relative thermal conductance $(G-G_0)/G_0$, where G_0 is the thermal conductance of heterostructures in the absence of mechanical loadings. Without water molecules (wt = 0), G increases by ~20% by 10% of ε_t . As the water content reaches 10%, G slightly increases with the tensile strain, and shows an enhancement similar to the one at wt = 0 at the water content of 25%. Figure 2b shows the relationship between G and the in-plane compressive strain ε_c . Without confined water molecules, G is approximately independent of ε_c . By contrast, at wt = 10% and 25%, the thermal conductance decreases with the increase of compressive strain, to approximately 90% of its initial value at $\,\varepsilon_{\rm c}\,$ of 20%. When a cross-plane pressure loading P is exerted on the GO layers, the heterostructure shows an enhanced thermal conductance G, as obtained in Figure 2c. As the water content increases, the enhancement remains but with a smaller ratio. With a cross-plane bending curvature κ applied to the heterostructure, Figure 2d shows that the thermal conductance without water molecules is slightly enhanced. When the water content increases to 10%, G increases by 10% at $\kappa = 0.06/\text{nm}$; at wt = 25%, the increase of G with bending curvature is significantly suppressed, leading to similar behavior to that of GO heterostructures without the confinement of water molecules.

3.2. Mechanism and generalized correlation between thermal conductance and H-bonds. To understand the underlying mechanism of the thermal response to mechanical

loadings, we first examine the atomic vibration features by investigating the phonon spectra. Under different mechanical loadings, **Figure 3a** shows no significant change in the phonon spectra of heterostructures, indicating negligible lattice deformation in the heterostructures, and thus phonon properties are barely changed.¹⁷ This non-change of phonon spectra of heterostructures is further confirmed under different loading levels with these four loading modes (**Figure S4**).

The strength of atomic interactions, as another physical parameter that is usually employed to understand the thermal transport at non-bonded molecular junctions, $^{18, 35}$ is then extracted and characterized by the interfacial interaction energy E_{int} . Figure 3b plots the variation of thermal conductance G with E_{int} . When there are no confined water molecules, a generalized linear relationship between G and E_{int} , independent of mechanical loading magnitude and modes, can be obtained, consistent with thermal transport across interfaces of bulk-bulk materials. $^{32, 36}$ When water molecules are introduced to the interlayer, although a higher E_{int} is obtained, the generalized linear relationship with the same slope between G and G and G and G are remains with a small deviation. This deviation becomes a little large at a high pressure loading and/or water content (25%) and is expected to be caused by the breaking of partial GO-GO interaction featured by functional groups and enhanced GO-water interactions, where the GO-water interactions suppress the thermal transport with Kapitza resistance by the contrasting vibration nature of atoms in GO and water. Similar results can be obtained in heterostructures with G and G and water.

Since the atomic interaction and interaction energy at non-bonded interfaces are essentially associated with H-bonds,³² the variation in the number of GO-GO and GO-W H-bonds are further investigated, as shown in the five subplots of **Figure 3c.** As the number of the confined water molecules increases, the number of GO-GO H-bonds decreases and the number of GO-W H-bonds increases (Figure 3c(i)), consistent with the thermal contributions to their corresponding G_{GO-GO} and G_{GO-W} in Figure 1d. With the increasing of in-plane tensile strain ε_t , the number of GO-GO H-bonds

increases at wt = 0%, but decreases with an increase in GO-W H-bonds at wt = 10%, which echoes with that of G_{GO-GO} and G_{GO-W} with ε_t in Figure S6a. At an in-plane compressive strain ε_c , the total number of H-bonds barely changes when there are no confined water molecules in the heterostructures (Figure 3c(ii)). On the other hand, at the water content of 10%, ε_c will lead to an increase in GO-W H-bonds and a decrease of GO-GO H-bonds (Figure 3c(iii)), which also agrees with that of G_{GO-GO} and G_{GO-W} with ε_c in **Figure S6b**. By contrast, when an out-of-plane pressure P is applied (Figure 3c(iv)), the number of both GO-GO and GO-W H-bonds at wt = 0and 10% will increase, corresponding to the increasing of G_{GO-GO} and G_{GO-W} in **Figure S6c.** The effect of bending curvature κ on H-bonds (Figure 3c(v)) indicates that larger κ lead to higher GO-GO and GO-W H-bonds. This increase will be larger at a higher wt, which is also confirmed by the thermal conductance in Figure S6d. With wt = 25%, similar results of H-bonds under these four loading modes are also obtained, as shown in Figure S7, indicating continuous agreement with the results of G_{GO-GO} and G_{GO-W} in Figure S6a-d. Figure 3d shows a generalized relationship between G and the number of H-bonds by considering water content wt as well as magnitudes and modes of mechanical loadings. A linear variation for both GO-GO and GO-W H-bonds is obtained but with a clearly different slope. The larger slope for GO-GO H-bonds indicates its higher contributions to thermal transport of heterostructures. The same generalized relationship is also obtained in the heterostructures with p = 0.4(Figure S8).

Afterward, to elucidate the role of H-bonds, **Figure 4a-e** shows the density distribution of H-bonds $\rho_{\rm HB}$ in the heterostructures with 10% of water ratio. Compared with the loading free condition in the heterostructure in Figure 4a, Figure 4b shows that an increase in tensile loading from 2.5% to 10% constrains the out-of-plane displacement of GO layers (**Figure S9a-b**), strengthening the confinement effect of water molecules and thus facilitating the formation and in-plane spread of GO-W H-bonds, yet leading to a slight reduction of GO-GO H-bonds. This distribution can be further confirmed from the planar area occupation rate ϕ of GO-W and GO-GO H-bonds.

bonds, where ϕ is defined as the ratio of the total planar occupation covered by the number of GO-W or GO-GO H-bonds to the total interlayer area of the heterostructure. The planar occupation of a single hydrogen bond can be estimated via $\pi r_{\rm HB}^2$ ($r_{\rm HB}=$ 0.24 nm is the cutoff distance of our employed OPLS-AA force field³³). compressive strain (Figure 4c), the formed GO-W H-bonds spread in the y-direction, leading to a larger region of GO-W H-bonds with the destruction of GO-GO H-bonds, which can be seen clearly in the plot of ϕ . Different from the constraint to the out-ofplane deformation under the tensile loading, the compression loading will promote an out-of-plane displacement and prevents the effective contact of GO-GO layers and GO layer-water (Figure S9c), which decreases the number of GO-GO H-bonds and also impedes the formation of GO-W H-bonds, leading to a smaller thermal conductance, as shown in Figure 2b. When an external pressure P is applied to the heterostructure, the interlay distance between GO layers will decrease (Figure S9d), leading to enhanced interactions including enhanced confinement effect of water molecules. Consequently, an increase in both GO-GO and GO-W H-bonding density is observed (Figure 4d). However, the formation of more GO-GO H-bonds leads to a higher ϕ meanwhile the ϕ of GO-W H-bonds remains, which indicates the external pressure does not spread the water in planar directions. The increase of both H-bonds becomes more obvious at a higher pressure, leading to an enhanced thermal conductance, as shown in Figure 2c. When the heterostructure is subjected to a mechanical bending, the interactions among water molecules will be weakened because of their interrupted (even discontinuous) distributions by bending deformation (Figure S9e), and GO-GO H-bonds will form, corresponding to the increased ϕ of GO-GO H-bonds (Figure 4e) and thus leading to a larger increase in thermal conductance (Figure 2d). As wt changes (e.g. 0 and 25%), the distribution and occupation rate ϕ of H-bonds with mechanical loadings will change correspondingly and has also been confirmed along with snapshots in Figure **S10-13**, consistent to the change in G (Figure 2).

3.3. Application of mechanical sensor design and demonstrations for multiple mechanical loading sensing and mode differentiation. The thermal transport

response of GO-water heterostructures to multiple mechanical loadings can be utilized as a sensor platform to distinguish mechanical modes that are commonly required in sensor design for applications in human-machine interfaces and smart e-skins. As a demonstration, a constant heat flow q is introduced to generate a temperature difference across the interface in the GO-water heterostructure with the water content of 10%, as illustrated in Figure 5a. Four typical mechanical loading modes, in-plane tension and compression and out-of-plane pressure and bending, are studied. The temperature difference between upper and lower graphene oxide layers ΔT will be measured as a parameter characterization for mechanical loading sensing and loading mode differentiation. For instance, with a tensile loading to the heterostructure, **Figure 5b** shows a continuous decrease of $(\Delta T - \Delta T_0)/\Delta T_0$, where ΔT_0 is the temperature difference in the absence of mechanical loading. By contrast, if the mechanical loading is an in-plane compression, $(\Delta T - \Delta T_0)/\Delta T_0$ shows a continuous increase (**Figure 5c**). The contrasting variation of temperature indicates that the in-plane tension and compression modes can be determined from the decreasing and increasing trend of temperature, respectively. Besides, the strain range can be as high as 10%, much higher than that of conventional strain sensors (usually less than 3%9), and can be used to sense a large mechanical strain. By analogy with electrical resistance-based strain sensors, we further define the gauge factor of this thermal property-based strain sensor via GF = $\frac{\Delta T - \Delta T_0}{\Delta T_0} / \varepsilon$, where ε is the applied in-plane strain, and GF is ~ 1 for both tension and compression, which is comparable with that of conventional strain sensors.³⁸⁻³⁹ It is expected that both the gauge factor and sensing range can be enhanced by programming the GO layers into meshed or kirigami structures. 17 When an out-of-plane pressure or bending is applied, Figure 5d and e show a continuous decrease of $(\Delta T - \Delta T_0)/\Delta T_0$ as the increasing of the pressure and bending curve, respectively, which is similar to that at tension. Further, the change rates of temperature difference can be used to identify the mechanical mode among tension, pressure and bending. For example, the external pressure leads to the fastest drop of temperature while there is the slowest one for the tension among these four types of mechanical loading modes. For comparison,

we designed a mechanical sensor enabled by heterostructure without water confined (i.e. wt=0) and performed the calculations. A similar change of temperature with that in the presence of confined water is observed to tensile, compression and bending modes, but the temperature remains unchanged to compression loading. This independence indicates that the compression loading mode cannot be sensed and results from the unchanged number of H-bonds (Figure 3c(iii)) due to the conformal attachment between GO layers under compression, which in turn confirms the critical role of confined water in the sensor design for mechanical model differentiation. In addition, extensive simulations on the sensor enabled by GO-water heterostructure under a small initial temperature drop ΔT_0 further confirm the robustness and sensitivity of sensing and differentiating these mechanical loading modes (**Figure S14**).

4. Conclusions

To reduce the effects of temperature variations and/or physical couplings associated with inputs of electrical power during measurements, mechanically flexible, structurally simple but functionally multiple sensors whose sensing mechanism does not rely on the electrical response are in the development to achieve comparable sensitivity. The structural design of sensors, from the packing and layer integration down to the nanoscale control and selection of materials microstructures, could yield unique response of underpinned properties to external mechanical loadings and environmental stimuli, thereby creating avenues for strategically extending sensor designs. We here provide a possibility by constructing a bilayer graphene-oxide heterostructure with liquid confined in the interlayer and report its unique thermal response to mechanical loading magnitudes and modes. Extensive atomistic modeling and comprehensive mechanism analysis elucidate the fundamental principle of solidliquid interaction in the confined interlayer spaces associated with dynamically reversible hydrogen bonding networks. The application demonstration of such solidconfined liquid heterostructures based mechanical sensors confirms that the mechanical loading sensing and mode differentiation to four typical mechanical modes, tension,

compression, pressure and bending can be realized from the measurement of the

temperature difference in the sensor. The results and findings extend a design solution

of mechanical sensors from electrical resistance based to thermal transport-based

responses. The employment of confined liquid and the resultant dynamic interactions

with solid components in response to external environments and stimuli foster the

opportunities for designing devices that currently rely on solid materials only.

Associate Content

Supporting Information

Comparison of van der Waals interaction and electrostatic interaction to thermal

transport. The separation distance between GO layers at different water contents.

Phonon spectra of graphene oxide under mechanical loadings. Thermal conductance

versus interfacial interaction energy. Decoupled thermal conductance along two heat

transfer paths. The decoupled relationship between the thermal conductance and the

number of H-bonds Deformation snapshots of heterostructures under mechanical

loadings. Planar distribution of H-bonds in the heterostructure. Measurement of relative

temperature with respect to an external mechanical loading at a lower heat flow.

Discussion of planar distribution of H-bonds under mechanical loadings.

Author Information

Corresponding Author

*Email: bx4c@virginia.edu.

ORCID

Yuan Gao: 0000-0001-6030-9497

Yue Zhang: 0000-0003-1429-724X

Baoxing Xu: 0000-0002-2591-8737

Notes

The authors declare no competing financial interest.

Acknowledgements

This work is supported by the start-up funds at the University of Virginia and NSF-

CBET-1805451. YG acknowledges the supports of John Bell McGaughy Fellowship. This work in part used the Extreme Science and Engineering Discovery Environment (XSEDE), which is supported by National Science Foundation grant number ACI-1548562.

Reference

- (1) Rogers, J. A. Wearable Electronics: Nanomesh on-Skin Electronics. *Nat. Nanotechnol.* **2017**, *12*, 839-840.
- (2) Hammock, M. L.; Chortos, A.; Tee, B. C. K.; Tok, J. B. H.; Bao, Z. 25th Anniversary Article: The Evolution of Electronic Skin (E-Skin): A Brief History, Design Considerations, and Recent Progress. *Adv. Mater.* **2013**, *25*, 5997-6038.
- (3) Dahiya, R. S.; Metta, G.; Valle, M.; Sandini, G. Tactile Sensing—from Humans to Humanoids. *IEEE Trans. Robot.* **2010**, *26*, 1-20.
- (4) Yeo, W. H.; Kim, Y. S.; Lee, J.; Ameen, A.; Shi, L.; Li, M.; Wang, S.; Ma, R.; Jin, S. H.; Kang, Z. Multifunctional Epidermal Electronics Printed Directly onto the Skin. *Adv. Mater.* **2013**, *25*, 2773-2778.
- (5) Liu, L.; Yu, Y.; Yan, C.; Li, K.; Zheng, Z. Wearable Energy-Dense and Power-Dense Supercapacitor Yarns Enabled by Scalable Graphene–Metallic Textile Composite Electrodes. *Nat. Commun.* **2015**, *6*, 7260.
- (6) Ha, M.; Lim, S.; Park, J.; Um, D. S.; Lee, Y.; Ko, H. Bioinspired Interlocked and Hierarchical Design of Zno Nanowire Arrays for Static and Dynamic Pressure-Sensitive Electronic Skins. *Adv. Funct. Mater.* **2015**, *25*, 2841-2849.
- (7) Pang, C.; Lee, G.-Y.; Kim, T.-i.; Kim, S. M.; Kim, H. N.; Ahn, S.-H.; Suh, K.-Y. A Flexible and Highly Sensitive Strain-Gauge Sensor Using Reversible Interlocking of Nanofibres. *Nat. Mater.* **2012**, *11*, 795-801.
- (8) Park, S.; Kim, H.; Vosgueritchian, M.; Cheon, S.; Kim, H.; Koo, J. H.; Kim, T. R.; Lee, S.; Schwartz, G.; Chang, H. Stretchable Energy-Harvesting Tactile Electronic Skin Capable of Differentiating Multiple Mechanical Stimuli Modes. *Adv. Mater.* **2014**, *26*, 7324-7332.
- (9) Kang, D.; Pikhitsa, P. V.; Choi, Y. W.; Lee, C.; Shin, S. S.; Piao, L.; Park, B.; Suh, K.-Y.; Kim, T.-i.; Choi, M. Ultrasensitive Mechanical Crack-Based Sensor Inspired by the Spider Sensory System. *Nature* **2014**, *516*, 222-226.
- (10) Muth, J. T.; Vogt, D. M.; Truby, R. L.; Mengüç, Y.; Kolesky, D. B.; Wood, R. J.; Lewis, J. A. Embedded 3d Printing of Strain Sensors within Highly Stretchable Elastomers. *Adv. Mater.* **2014**, *26*, 6307-6312.
- (11) Trung, T. Q.; Ramasundaram, S.; Hwang, B. U.; Lee, N. E. An All-Elastomeric Transparent and Stretchable Temperature Sensor for Body-Attachable Wearable Electronics. *Adv. Mater.* **2016**, *28*, 502-509.
- (12) Liao, A. D.; Wu, J. Z.; Wang, X.; Tahy, K.; Jena, D.; Dai, H.; Pop, E. Thermally Limited Current Carrying Ability of Graphene Nanoribbons. *Phys. Rev. Lett.* **2011**, *106*, 256801.

- (13) Geim, A. K.; Grigorieva, I. V. Van Der Waals Heterostructures. *Nature* **2013**, *499*, 419-425, DOI: 10.1038/nature12385.
- (14) Li, M.-Y.; Chen, C.-H.; Shi, Y.; Li, L.-J. Heterostructures Based on Two-Dimensional Layered Materials and Their Potential Applications. *Mater. Today* **2016**, *19*, 322-335.
- (15) Akinwande, D.; Petrone, N.; Hone, J. Two-Dimensional Flexible Nanoelectronics. *Nat. Commun.* **2014**, *5*, 5678.
- (16) Choi, M. S.; Lee, G.-H.; Yu, Y.-J.; Lee, D.-Y.; Lee, S. H.; Kim, P.; Hone, J.; Yoo, W. J. Controlled Charge Trapping by Molybdenum Disulphide and Graphene in Ultrathin Heterostructured Memory Devices. *Nat. Commun.* **2013**, *4*, 1624.
- (17) Gao, Y.; Yang, W.; Xu, B. Tailoring Auxetic and Contractile Graphene to Achieve Interface Structures with Fully Mechanically Controllable Thermal Transports. *Adv. Mater.* **2017**, *4*, 1700278.
- (18) Gao, Y.; Xu, B. On the Generalized Thermal Conductance Characterizations of Mixed One-Dimensional—Two-Dimensional Van Der Waals Heterostructures and Their Implication for Pressure Sensors. *ACS Appl. Mater. Interfaces* **2018**, *10*, 14221-14229.
- (19) Wan, S.; Peng, J.; Li, Y.; Hu, H.; Jiang, L.; Cheng, Q. Use of Synergistic Interactions to Fabricate Strong, Tough, and Conductive Artificial Nacre Based on Graphene Oxide and Chitosan. *ACS Nano* **2015**, *9*, 9830-9836.
- (20) Borini, S.; White, R.; Wei, D.; Astley, M.; Haque, S.; Spigone, E.; Harris, N.; Kivioja, J.; Ryhanen, T. Ultrafast Graphene Oxide Humidity Sensors. *ACS Nano* **2013**, 7, 11166-11173.
- (21) Plimpton, S. Fast Parallel Algorithms for Short-Range Molecular Dynamics. *J. Comput. Phys.* **1995**, *117*, 1-19.
- (22) Jorgensen, W. L.; Maxwell, D. S.; Tirado-Rives, J. Development and Testing of the Opls All-Atom Force Field on Conformational Energetics and Properties of Organic Liquids. *J. Am. Chem. Soc.* **1996**, *118*, 11225-11236.
- (23) Wan, J.; Jiang, J.-W.; Park, H. S. Negative Poisson's Ratio in Graphene Oxide. *Nanoscale* **2017**, *9*, 4007-4012.
- (24) Zhao, W.; Wang, Y.; Wu, Z.; Wang, W.; Bi, K.; Liang, Z.; Yang, J.; Chen, Y.; Xu, Z.; Ni, Z. Defect-Engineered Heat Transport in Graphene: A Route to High Efficient Thermal Rectification. *Sci. Rep.* **2015**, *5*, 11962.
- (25) Mark, P.; Nilsson, L. Structure and Dynamics of the Tip3p, Spc, and Spc/E Water Models at 298 K. J. Phys. Chem. A 2001, 105, 9954-9960.
- (26) Medhekar, N. V.; Ramasubramaniam, A.; Ruoff, R. S.; Shenoy, V. B. Hydrogen Bond Networks in Graphene Oxide Composite Paper: Structure and Mechanical Properties. *ACS Nano* **2010**, *4*, 2300-2306.
- (27) Balasubramanian, G.; Puri, I. K. J. A. P. L. Heat Conduction across a Solid-Solid Interface: Understanding Nanoscale Interfacial Effects on Thermal Resistance. **2011**, *99*, 013116.
- (28) Hou, D.; Yang, T. J. P. C. C. P. A Reactive Molecular Dynamics Study of Graphene Oxide Sheets in Different Saturated States: Structure, Reactivity and Mechanical Properties. **2018**, *20*, 11053-11066.
- (29) Cao, C.; Daly, M.; Chen, B.; Howe, J. Y.; Singh, C. V.; Filleter, T.; Sun, Y. J. N. 1.

- Strengthening in Graphene Oxide Nanosheets: Bridging the Gap between Interplanar and Intraplanar Fracture. **2015**, *15*, 6528-6534.
- (30) Zhang, D.-B.; Akatyeva, E.; Dumitrică, T. Bending Ultrathin Graphene at the Margins of Continuum Mechanics. *Phys. Rev. Lett.* **2011**, *106*, 255503.
- (31) Xiong, S.; Cao, G. Bending Response of Single Layer Mos2. *Nanotechnology* **2016**, *27*, 105701.
- (32) Zhang, T.; Gans-Forrest, A. R.; Lee, E.; Zhang, X.; Qu, C.; Pang, Y.; Sun, F.; Luo, T. Role of Hydrogen Bonds in Thermal Transport across Hard/Soft Material Interfaces. *ACS Appl. Mater. Interfaces* **2016**, *8*, 33326-33334.
- (33) Willcox, J. A.; Kim, H. J. Molecular Dynamics Study of Water Flow across Multiple Layers of Pristine, Oxidized, and Mixed Regions of Graphene Oxide. *ACS Nano* **2017**, *11*, 2187-2193.
- (34) Xu, B.; Li, Y.; Park, T.; Chen, X. Effect of Wall Roughness on Fluid Transport Resistance in Nanopores. *J. Chem. Phys.* **2011**, *135*, 144703.
- (35) Gao, Y.; Xu, B. Van Der Waals Graphene Kirigami Heterostructure for Strain-Controlled Thermal Transparency. *ACS Nano* **2018**, *12*, 11254-11262.
- (36) Shenogina, N.; Godawat, R.; Keblinski, P.; Garde, S. How Wetting and Adhesion Affect Thermal Conductance of a Range of Hydrophobic to Hydrophilic Aqueous Interfaces. *Phys. Rev. Lett.* **2009**, *102*, 156101.
- (37) Alexeev, D.; Chen, J.; Walther, J. H.; Giapis, K. P.; Angelikopoulos, P.; Koumoutsakos, P. Kapitza Resistance between Few-Layer Graphene and Water: Liquid Layering Effects. *Nano Lett.* **2015**, *15*, 5744-5749.
- (38) Shin, U.-H.; Jeong, D.-W.; Park, S.-M.; Kim, S.-H.; Lee, H. W.; Kim, J.-M. Highly Stretchable Conductors and Piezocapacitive Strain Gauges Based on Simple Contact-Transfer Patterning of Carbon Nanotube Forests. *Carbon* **2014**, *80*, 396-404.
- (39) Yao, S.; Zhu, Y. Wearable Multifunctional Sensors Using Printed Stretchable Conductors Made of Silver Nanowires. *Nanoscale* **2014**, *6*, 2345-2352.

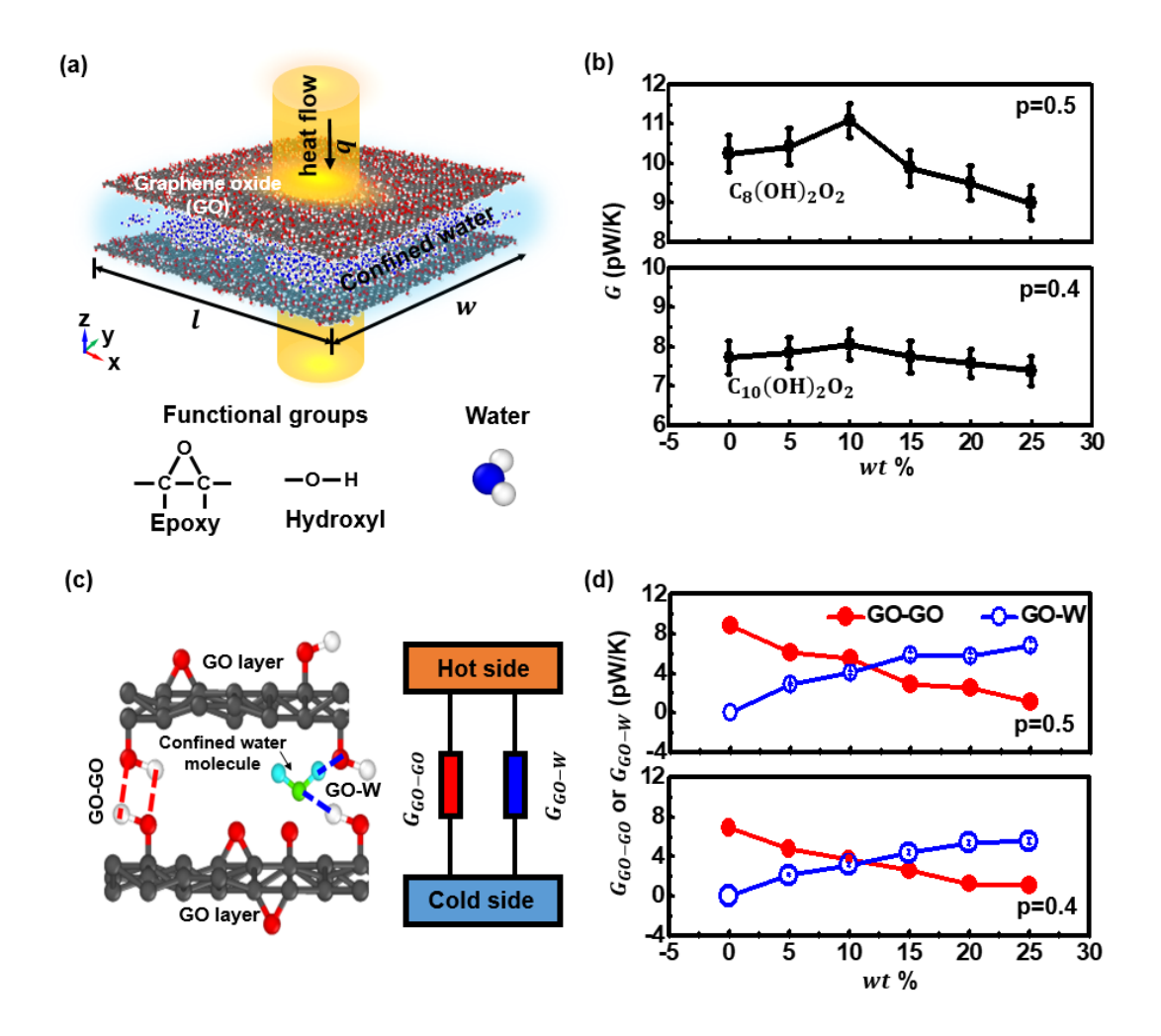


Figure 1. Thermal conductance of graphene oxide (GO)-confined water heterostructures. (a) Atomistic modeling of the graphene oxide (GO)-confined water heterostructure with the size of l = 6.15 nm and w = 6.39 nm. The surface of both GO layers that is decorated with epoxy and hydroxyl functional groups reflects the oxidation. The heat is transferred from upper graphene oxide layer to the lower one. (b) Thermal conductance G of the heterostructures with a degree of oxidation p = 0.4 and 0.5 as functions of confined water content. (c) Schematic of the hydrogen bondsfeatured interactions between graphene oxide layers (GO-GO) and between graphene oxide and water molecules (GO-W) (left) and their correspondence to a circuit model consisting of the two heat transfer paths with thermal conductance of $G_{\rm GO-GO}$ and $G_{\rm GO-W}$, respectively (right). (d) Variation of $G_{\rm GO-GO}$ and $G_{\rm GO-W}$ as functions of water content in the heterostructure with a degree of oxidation p = 0.4 and 0.5.

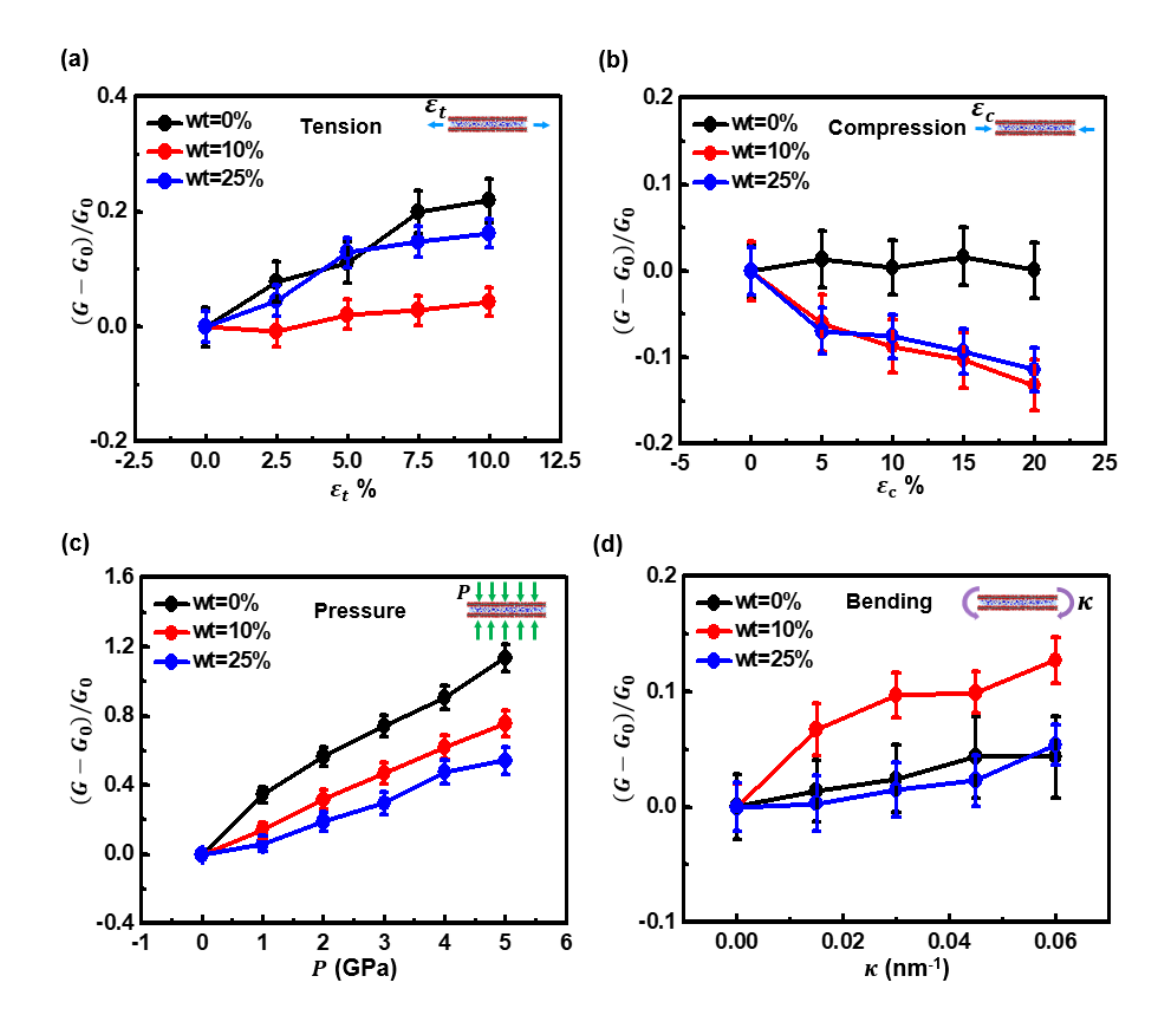


Figure 2. Responses of thermal conductance in graphene oxide (GO)-confined water heterostructures to different mechanical loading modes. The thermal conductance G in the heterostructure with a degree of oxidation p=0.5 and water content of 0, 10% and 25% as functions of (a) in-plane tensile strain ε_t , (b) in-plane compressive strain ε_c , (c) cross-plane pressure P and (d) cross-plane bending curvature κ .

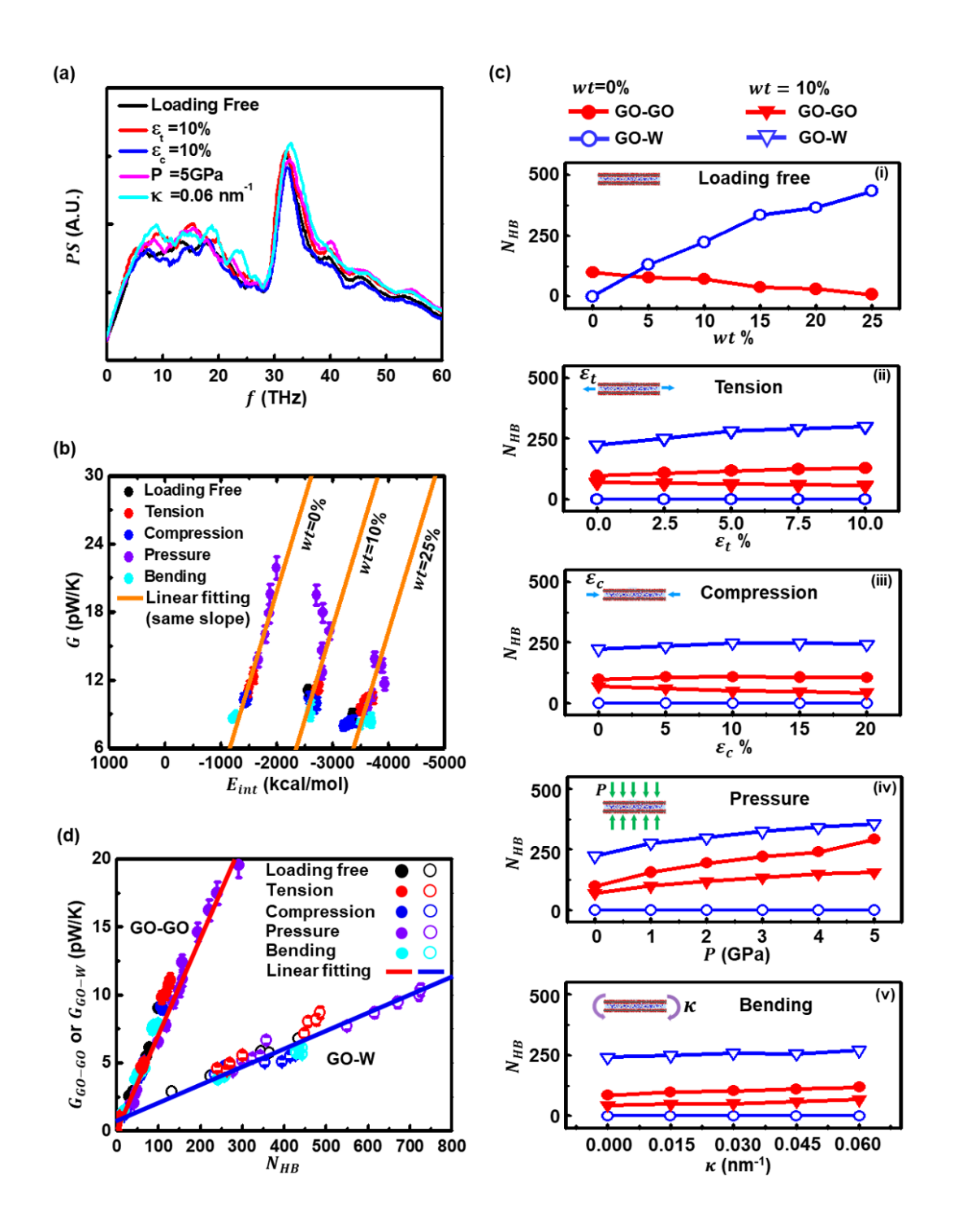


Figure 3. Thermal transport mechanism and correlation with hydrogen bonds. (a) Phonon spectra of graphene oxide under mechanical loadings of tension, compression, pressure and bending. (b) Thermal conductance G versus interfacial interaction energy E_{int} . (c) The number of hydrogen (H)-bonds between graphene oxide (GO-GO H-bonds) and graphene oxide and water (GO-W H-bonds) as functions of (i) water content, (ii) tensile strain ε_t , (iii) compressive strain ε_c , (iv) external pressure P, and (v) bending curvature κ . (d) Decoupled contribution of GO-GO H-bonds to thermal conductance $G_{\text{GO-GO}}$ and GO-W H-bonds to thermal conductance $G_{\text{GO-W}}$.

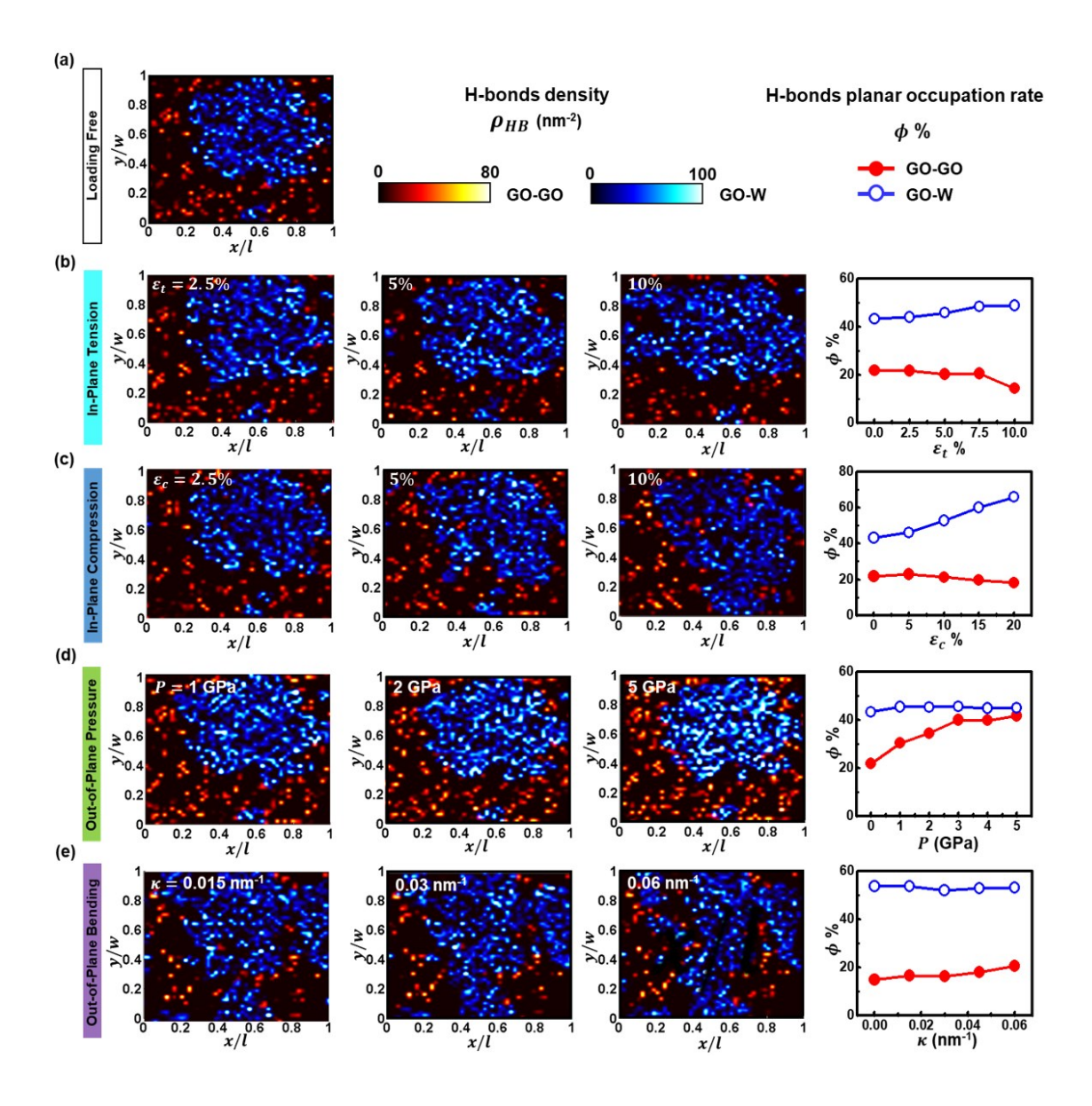


Figure 4. Planar distribution and occupation of hydrogen (H)-bonds in the interlayer of confined water and graphene oxide. The density $\rho_{\rm HB}$ and planar occupation rate ϕ of hydrogen bonds in the interlayer of heterostructures with degree of oxidation p=0.5 and water weight ratio wt=10% (a) in the absence of loading, under (b) tensile strain $\varepsilon_{\rm t}$, (c) compressive strain $\varepsilon_{\rm c}$, (d) external pressure P, and (e) bending curvature κ . The H-bonds formed between graphene oxide layers (GO-GO) and between graphene oxide and water molecules (GO-W) are represented by red and blue dots, respectively.

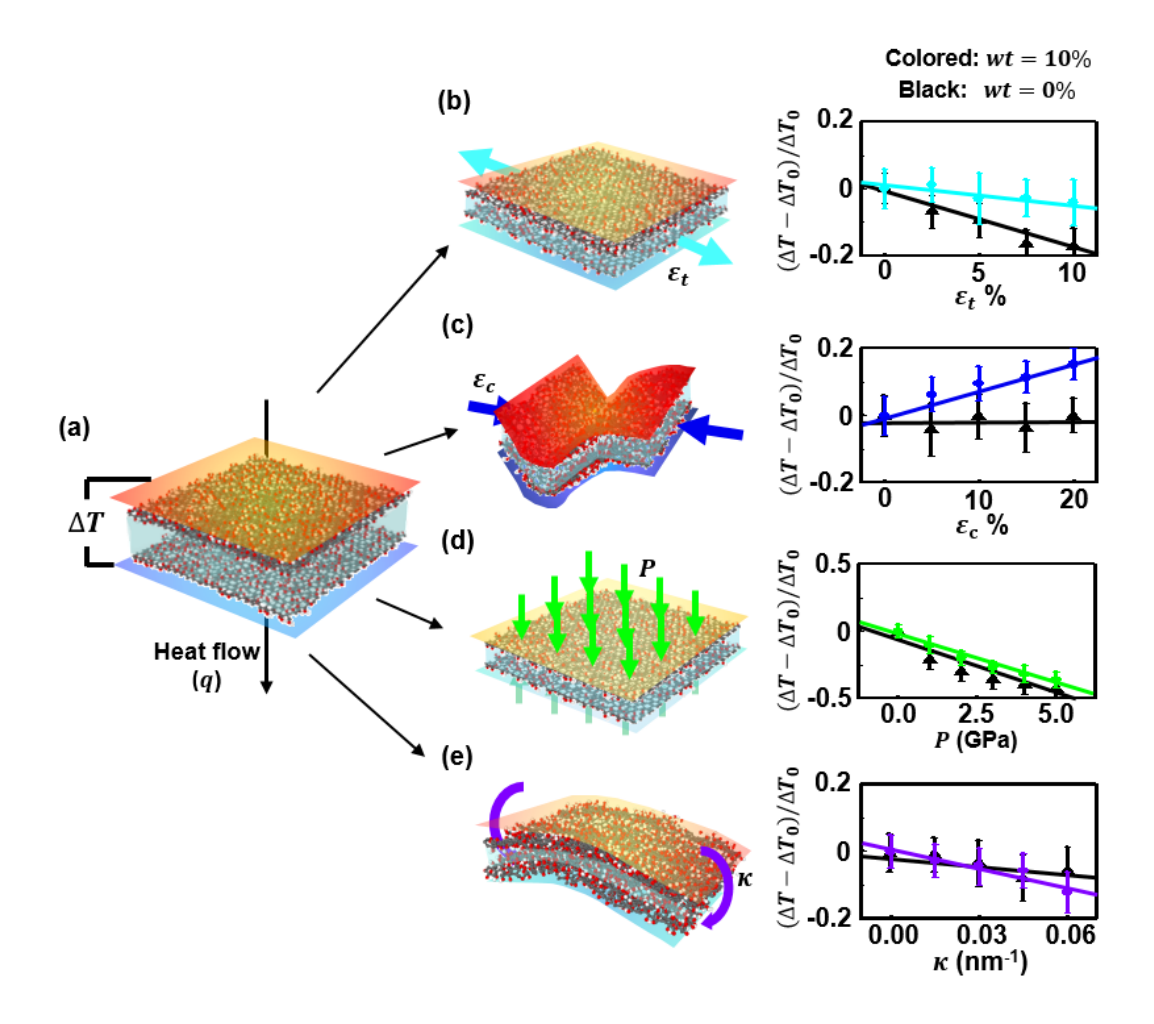


Figure 5. Design and demonstration application of mechanical sensor enabled by graphene oxide-confined water heterostructure. (a) Schematic of mechanical sensor design, where a constant heat flow q is applied to generate a temperature difference ΔT between the graphene oxides in the heterostructure. Measurement of relative temperature $(\Delta T - \Delta T_0)/T_0$ with respect to external mechanical loadings of (b) tension ε_t , (c) compression ε_c , (d) pressure P and (e) bending curvature κ . ΔT (~60 K) is the temperature difference in the absence of mechanical loading.

TOC

